

Ethane Oxidative Dehydrogenation Pathways on Vanadium Oxide Catalysts

Morris D. Argyle, Kaidong Chen,[†] Alexis T. Bell,* and Enrique Iglesia*

Chemical Sciences Division, E. O. Lawrence Berkeley National Laboratory, and Department of Chemical Engineering, University of California, Berkeley, California 94720-1462

Received: December 10, 2001

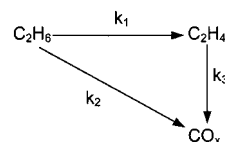
Kinetic and isotopic tracer and exchange measurements were used to determine the identity and reversibility of elementary steps involved in ethane oxidative dehydrogenation (ODH) on $\text{VO}_x/\text{Al}_2\text{O}_3$ and VO_x/ZrO_2 . C_2H_6 – C_2D_6 – O_2 and C_2H_6 – D_2O – O_2 react to form alkenes and CO_x without concurrent formation of $\text{C}_2\text{H}_{6-x}\text{D}_x$ or $\text{C}_2\text{H}_{4-x}\text{D}_x$ isotopomers, suggesting that C–H bond cleavage in ethane and ethene is an irreversible and kinetically relevant step in ODH and combustion reactions. Primary ethane ODH reactions show normal kinetic isotopic effects ($k_{\text{C-H}}/k_{\text{C-D}} = 2.4$); similar values were measured for ethane and ethene combustion (1.9 and 2.8, respectively). $^{16}\text{O}_2$ – $^{18}\text{O}_2$ – C_2H_6 reactions on supported V^{16}O_x domains led to the initial appearance of ^{16}O from the lattice in H_2O , CO , and CO_2 , consistent with the involvement of lattice oxygen in C–H bond activation steps. Isotopic contents are similar in H_2O , CO , and CO_2 , suggesting that ODH and combustion reactions use similar lattice oxygen sites. No $^{16}\text{O}^{18}\text{O}$ isotopomers were detected during reactions of $^{16}\text{O}_2$ – $^{18}\text{O}_2$ – C_2H_6 mixtures, as expected if dissociative O_2 chemisorption steps were irreversible. The alkyl species formed in these steps desorb irreversibly as ethene and the resulting O–H groups recombine to form H_2O and reduced V centers in reversible desorption steps. These reduced V centers reoxidize by irreversible dissociative chemisorption of O_2 . A pseudo-steady state analysis of these elementary steps together with these reversibility assumptions led to a rate expression that accurately describes the observed inhibition of ODH rates by water and the measured kinetic dependence of ODH rates on C_2H_6 and O_2 pressures. This kinetic analysis suggests that surface oxygen, OH groups, and oxygen vacancies are the most abundant reactive intermediates during ethane ODH on active VO_x domains.

Introduction

Oxidative dehydrogenation (ODH) provides an exothermic and thermodynamically favored route to ethene using ethane as the reactant. The formation of water overcomes the thermodynamic hurdles and the high temperatures involved in non-oxidative thermal or catalytic routes to ethene. Many previous studies have examined several metal oxides as catalysts^{1–11} and VO_x -based materials are among the most active and selective catalysts for ethane ODH. Ethane ODH reactions occur in parallel with ethane combustion and with combustion of the ethene formed in primary ODH steps (Scheme 1). These pathways lead to the observed effects of reactor residence time on reaction rate and selectivity.¹¹ In Scheme 1, k_1 , k_2 , and k_3 represent pseudo-first-order rate constants for ethane oxidative dehydrogenation, ethane combustion, and ethene combustion, respectively. Several other reaction schemes and mechanisms have been proposed for ethane ODH on vanadia and other active oxides.^{1–9} Previous studies on VO_x - SiO_2 have provided the most detailed mechanistic picture for ethane reactions,^{6–9} but for catalysts leading to more complex reaction products, including acetone and acetaldehyde.

Previous reports have based their mechanistic conclusions on the kinetic dependence of these reactions on C_2H_6 and O_2 , without independent evidence from isotopic tracer or exchange studies for the role of lattice oxygen and for the reversibility or

SCHEME 1: Primary and Secondary Reaction Pathways in Oxidative Dehydrogenation of Ethane



kinetic relevance of specific elementary steps. Such details have been recently reported for propane ODH reactions on supported VO_x , MoO_x , and WO_x .^{12–14} Both primary and secondary reactions were shown to proceed via Mars-van Krevelen¹⁵ pathways involving lattice oxygen atoms, which are removed and restored during each catalytic turnover.

Here, we report isotopic tracer and exchange studies of ethane dehydrogenation and combustion pathways $\text{VO}_x/\text{Al}_2\text{O}_3$ and VO_x/ZrO_2 catalysts. A sequence of elementary steps consistent with ethane ODH kinetic data was confirmed by isotopic tracer and exchange measurements and by kinetic isotope effects obtained from relative rate constants measured for each of the three rate constants in Scheme 1 using C_2H_6 – O_2 and C_2D_6 – O_2 mixtures ($k_{\text{nH}}/k_{\text{nD}}$). The rate expression derived from the proposed catalytic sequence accurately describes ethane ODH rates on $\text{VO}_x/\text{Al}_2\text{O}_3$, VO_x/ZrO_2 , and unsupported V_2O_5 catalysts.

Experimental Section

$\text{VO}_x/\text{Al}_2\text{O}_3$ catalysts were prepared by incipient wetness impregnation of γ -alumina (Degussa, AG, 100 m^2/g) with aqueous solutions of ammonium metavanadate containing also

* To whom correspondence should be addressed [E-mail: iglesias@cchem.berkeley.edu; bell@cchem.berkeley.edu].

[†] Current address: General Electric Corporation, 1 Research Circle, GECD, CEB 417, Niskayuna, New York 12309.

TABLE 1: Surface Area and V Surface Density for VO_x Catalysts

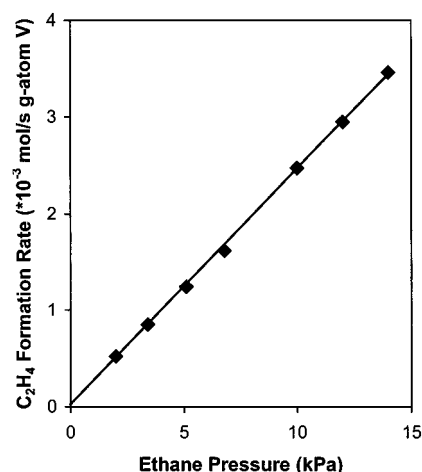
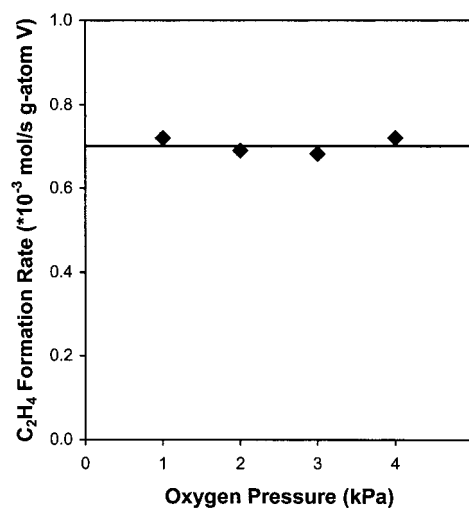
V ₂ O ₅ loading (wt %)	surface area (m ² /g)	nominal VO _x surface density (V/nm ²)
2 V ₂ O ₅ /Al ₂ O ₃	95	1.4
10 V ₂ O ₅ /Al ₂ O ₃	83	8.0
30 V ₂ O ₅ /Al ₂ O ₃	58	34.2
10 V ₂ O ₅ /ZrO ₂	170	3.9

oxalic acid. The impregnated samples were dried, crushed, treated in dry air at 773 K, and sieved to retain 180–355 μm particles. Catalyst synthesis and structural characterization procedures and the results were reported previously.¹¹ VO_x/ZrO₂ catalysts were prepared similarly using Zr oxyhydroxide powders as supports.^{16,17} Table 1 shows surface areas and nominal vanadia surface densities for the catalysts.

The effects of reactant and product concentrations on reaction rates and rate constants were measured using a packed-bed flow reactor with plug-flow hydrodynamics. VO_x/Al₂O₃ and VO_x/ZrO₂ catalysts (0.01–0.3 g, 180–355 μm) and V₂O₅ powders (Johnson Matthey, 99.9%, 0.49–0.78 g, <355 μm) were diluted with quartz granules (180–355 μm, 0.01–0.3 g) in order to prevent temperature gradients and to ensure plug-flow hydrodynamics. No products were detected on Al₂O₃, ZrO₂, quartz chips, or an empty reactor at the conditions of this study. Reaction rates were measured on VO_x/ZrO₂ (3.9 V/nm²) at ethane pressures of 2–15 kPa and O₂ pressures of 1–4 kPa. Kinetic inhibition by products was probed by adding up to 10 kPa H₂O and 1 kPa CO_x (CO₂: Liquid Carbonic, 50.3%, balance N₂; CO: Praxair, 2%, balance He) to the feed. H₂O was introduced by flowing H₂ (Airgas, 99.99%) over a CuO bed (100 g, 13 wt % CuO/Al₂O₃) at 623 K in order to convert all the H₂ to H₂O. All transfer lines after H₂O introduction were kept at ~400 K. Kinetic measurements were also carried out on three VO_x/Al₂O₃ samples with surface densities of 1.4, 8.0, and 34 V/nm². In these measurements, the C₂H₆ pressure was kept at 14 kPa and O₂ partial pressures were varied (1.7–6.8 kPa) in order to achieve C₂H₆/O₂ ratios of 2–8. The C₂H₆ pressure was changed to 3.4 kPa and then to 6.8 kPa, while keeping the O₂ pressure at 1.7 kPa. C₂H₆ (Scott Specialty Gases, research grade, >99.999%) and O₂ (Praxair, research grade, chemical purity >99.999%) were used without further purification in all experiments. Helium (Airgas, research grade >99.9999%) was used as an inert diluent.

Typical C₂H₆ and O₂ conversions were 1–2% and 10–20%, respectively. A Hewlett-Packard 6890 gas chromatograph equipped with packed (Supelco Carboxen 1004) and capillary (HP-1, 50 m, 320 μm) columns and thermal conductivity and flame ionization detectors was used to measure reactant and product concentrations in the effluent stream. The reaction temperature was varied between 663 and 743 K and reactor residence times were adjusted by varying ethane molar flow rates between 0.017 and 0.17 mol/s g-atom V. Reaction rate data as a function of residence time were used in order to calculate initial rates for primary dehydrogenation and combustion reactions and each of the rate constants in Scheme 1.¹¹

Isotopic studies were conducted using a gradientless recirculating batch reactor with catalyst samples (~0.1 g) held in a shallow bed at 663 K.¹⁸ Gradientless operation was ensured by keeping C₂H₆ and O₂ conversions below 1% per pass. Reactants were introduced into the recirculating volume (400 cm³) after evacuation to <0.1 Pa. A graphite gear pump was used to circulate reactor contents at 1.67 cm³ s⁻¹. The chemical and isotopic compositions of reactants and products were measured by injecting gas samples into a gas chromatograph equipped

**Figure 1.** Effect of C₂H₆ concentration on C₂H₄ formation rate on 10 wt % V₂O₅/ZrO₂ (3.9 V/nm²) [1.7 kPa O₂, balance He, 723 K].**Figure 2.** Effect of O₂ concentration on C₂H₄ formation rate on 10 wt % V₂O₅/ZrO₂ (3.9 V/nm²) [3.4 kPa C₂H₆, balance He, 723 K].

with a mass selective detector (Hewlett-Packard 5872). The ion yields were analyzed using deconvolution methods that account for natural ¹³C abundance and fragmentation patterns¹⁹ in order to obtain the ¹³C, ²H, and ¹⁸O isotopomer distributions in each reactant or product. C₂H₆ (Scott Specialty Gases, research grade, >99.999%), C₂D₆ (Isotec, chemical purity >99%, isotopic purity >99%), ¹³C₂H₄ (Isotec, chemical purity >99.9%, isotopic purity >99%), ¹⁶O₂ (Praxair, research grade, chemical purity >99.999%, isotopic purity 99.92%), ¹⁸O₂ (Isotec, chemical purity >99%, isotopic purity >99%), and ²H₂O (Isotec, chemical purity 100%, isotopic purity 99.9%), were used without further purification. Helium (Airgas, research grade >99.9999%) was used as an inert diluent.

Results and Discussion

Effects of Reactant and Product Concentrations on Reaction Rates. Figures 1, 2, and 3 show primary ethane ODH rates (from residence time data extrapolated to zero conversion) as a function of reactant and product concentrations on 10 wt % V₂O₅/ZrO₂ (3.9 V/nm²). Dehydrogenation rates were nearly first-order in C₂H₆ (Figure 1) and almost zero order in O₂ (Figure 2). The addition of water decreased primary C₂H₆ dehydrogenation rates (Figure 3). These inhibition effects weakened with increasing H₂O concentration, as also reported previously on VO_x/SiO₂.¹⁰ Neither CO nor CO₂ influenced primary ODH rates

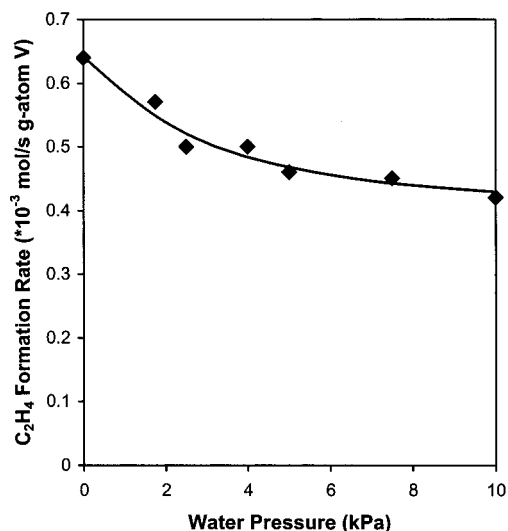
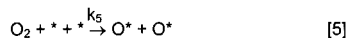
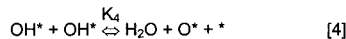
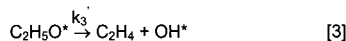
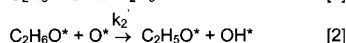
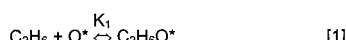


Figure 3. Effect of H₂O concentration on C₂H₄ formation rate on 10 wt % V₂O₅/ZrO₂ (3.9 V/nm²) [3.4 kPa C₂H₆, 1.7 kPa O₂, balance He, 723 K].

SCHEME 2: Sequence of Elementary Steps and Derived Rate Equation for Oxidative Dehydrogenation of Ethane on VO_x Catalysts



$$r_{\text{C}_2\text{H}_4} = \frac{K_1 k_2' [\text{C}_2\text{H}_6]}{\{1 + ([\text{H}_2\text{O}]/K_4)^{0.5} (K_1 k_2' [\text{C}_2\text{H}_6])^{0.25} / (2k_5 [\text{O}_2])^{0.25} + (K_1 k_2' [\text{C}_2\text{H}_6])^{0.5} / (2k_5 [\text{O}_2])^{0.5}\}^2}$$

$$= \frac{k_{\text{eff}} [\text{C}_2\text{H}_6]}{\{1 + \alpha [\text{H}_2\text{O}]^{0.5} [\text{C}_2\text{H}_6]^{0.25} / [\text{O}_2]^{0.25} + \beta [\text{C}_2\text{H}_6]^{0.5} / [\text{O}_2]^{0.5}\}^2} \quad [6]$$

on VO_x/ZrO₂. Similar conclusions were reached on the other VO_x/Al₂O₃ catalysts studied, indicating that ethane ODH reaction orders on VO_x domains are not influenced by the support or by any changes in domain size or structure caused by changes in the support or in the VO_x surface density. Detailed kinetic measurements on VO_x/ZrO₂ and VO_x/Al₂O₃ were consistent with ethane orders slightly smaller than one and with small positive orders in O₂ concentration. This kinetic dependence reflects some subtle mechanistic details illustrated by the elementary steps in Scheme 2; it is significantly more complex than the zero and first-order respective O₂ and C₂H₆ dependences widely reported for alkane ODH reactions.^{1–4}

Scheme 2 shows a set of elementary steps consistent with this kinetic dependence and with the isotopic experiments reported below. O* represents a lattice oxygen (O=V, V–O–V, or V–O–M, where M is the oxide support). C₂H₅O* is an ethoxide species attached to a V-cation (C₂H₅–O–V); OH* denotes a hydroxyl group bound to V or M, and * is a reduced V center, consisting of an oxygen vacancy at a single V³⁺ or shared between two V⁴⁺. Step 1 represents the quasi-equilibrated weak molecular adsorption of ethane. In this Scheme, Step 2 becomes the only kinetically relevant step when O* is the most abundant reactive intermediate (*mar*). This step involves the activation of one of the six equivalent C–H bonds in ethane using lattice oxygens to form an adsorbed ethoxide species and

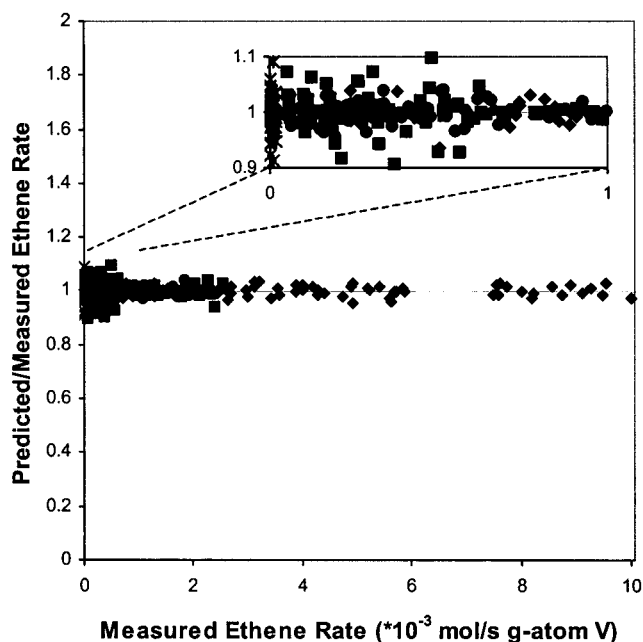


Figure 4. Predicted versus actual rates of ethane ODH on VO_x/Al₂O₃ and V₂O₅ using the rate equation in Scheme 2; squares: 2 wt % V₂O₅/Al₂O₃ (1.4 V/nm²); diamonds: 10 wt % V₂O₅/Al₂O₃ (8.0 V/nm²); circles: 30 wt % V₂O₅/Al₂O₃ (34 V/nm²); stars: unsupported V₂O₅; [3.4–14 kPa C₂H₆, 1.7–6.8 kPa O₂, 663–743 K].

an OH group. These ethoxide species then form ethene in Step 3, via the elimination of an H atom to form a second OH group. Step 4 involves the quasi-equilibrated recombination of two vicinal OH groups to form water, leaving behind an oxygen vacancy. The irreversible dissociative chemisorption of O₂ (Step 5) then reoxidizes the reduced V centers to form the stoichiometric V⁵⁺ oxide domains required for a new catalytic cycle. This Mars-van Krevelen mechanism resembles those shown to account for propane ODH on VO_x¹² and MoO_x¹⁴ catalysts.

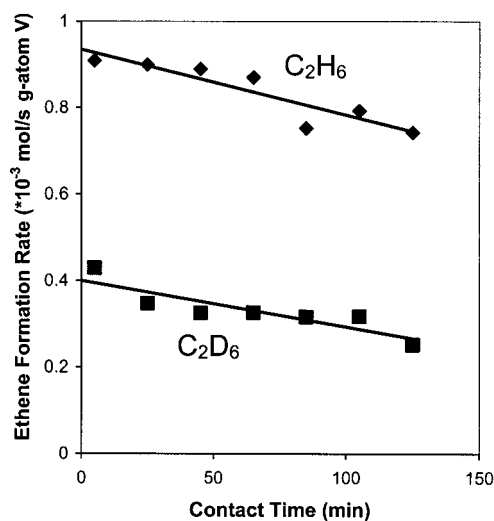
The elementary steps shown in Scheme 2 lead to the rate equation shown in eq 6 (Scheme 2). This rate equation follows from Scheme 2 via the straightforward application of the pseudosteady-state hypothesis (PSSH) for each surface species together with the quasi-equilibrium assumption for steps 1 and 4, and the assumption of O*, OH*, and * as the most abundant reactive intermediates (*mar*). This equation accurately describes the experimental rate data, including the apparent deviations of the C₂H₆ and O₂ orders from 1 and 0, respectively, as shown by the comparison between the predictions from these equations and the measured reaction rates included in Figure 4. Thus, the mechanism shown in Scheme 2 is consistent with experimental rate measurements. Ethane ODH rates per V on both 2 wt % V₂O₅/Al₂O₃ and unsupported V₂O₅ (squares and stars visible in the Figure 4 inset) are very low, and they lead to less accurate flow and conversion measurements and to more scatter for these rate measurements than for those on 10 wt % and 30 wt % V₂O₅/Al₂O₃ catalysts.

The values of the parameters used in the ethane ODH rate equation (eq 6) for 10 wt % V₂O₅/Al₂O₃ (Figure 4) are given in Table 2. The ethane adsorption equilibrium constant, K₁, and the initial C–H bond activation rate constant, k'₂, appear as an effective rate constant (k_{eff}) in the numerator of eq 6. The values of k_{eff} follow the expected Arrhenius-type magnitude increase with increasing reaction temperature. Its apparent activation energy is 110 (±15) kJ/mol, in agreement with previous measurements on this catalyst.¹¹ The three terms in the denominator of eq 6 reflect the relative contributions of O*,

TABLE 2: Values of Fitted Kinetic Parameters for the Ethane ODH Rate Equation (Eq 6 in Scheme 2)

parameter	663 K	683 K	703 K	723 K	743 K
k_{eff}^d ($\text{cm}^3 \text{mol}^{-1} \text{s}^{-1}$)	30	50	91	150	240
α^b ($\text{cm}^{1.5} \text{mol}^{-0.5} \text{s}^{-0.5}$)	14	3.3	0	0	0
$\alpha[\text{C}_2\text{H}_6]^{0.25}[\text{H}_2\text{O}]^{0.5}[\text{O}_2]^{-0.25}$ ^c	0.09	0.02	0	0	0
typical values					
β^d	0.06	0.06	0.07	0.06	0.04
$\beta[\text{C}_2\text{H}_6]^{0.5}[\text{O}_2]^{-0.5}$ ^e	0.02	0.02	0.02	0.02	0.01
typical values					

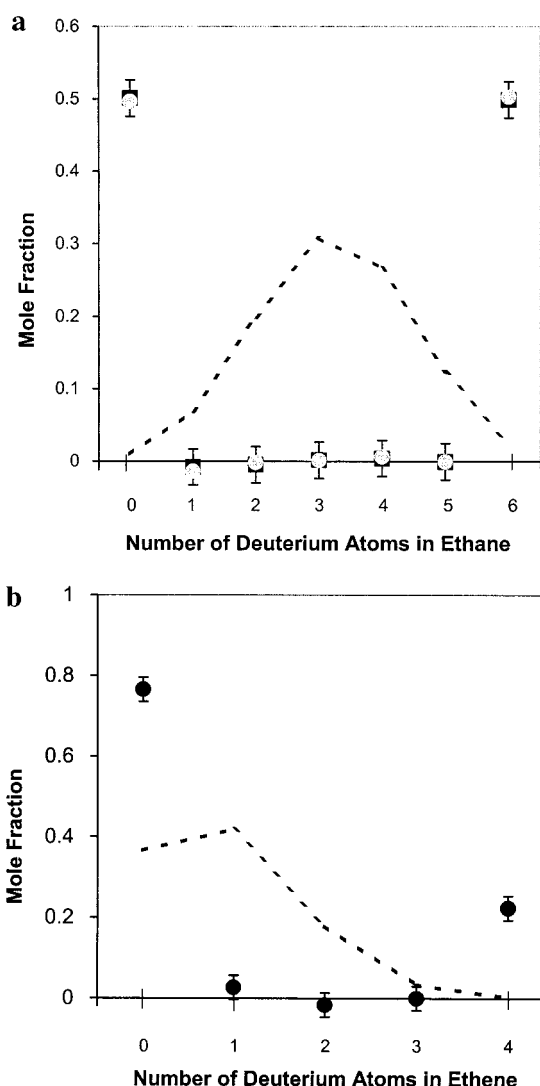
$$a = K_1 k'_2, \quad b = K_1^{0.25} k'_2^{0.25} K_4^{-0.5} 2k_5^{-0.25}, \quad c = (K_1 k'_2 [\text{C}_2\text{H}_6])^{0.25} ([\text{H}_2\text{O}] / K_4)^{0.5} (2k_5 [\text{O}_2])^{-0.25}, \quad d = K_1^{0.5} k'_2^{0.5} 2k_5^{-0.5}, \quad e = (K_1 k'_2 [\text{C}_2\text{H}_6])^{0.5} (2k_5 [\text{O}_2])^{-0.5}.$$

**Figure 5.** Ethene formation rate as a function of time during ethane ODH with C_2H_6 and with C_2D_6 reactants on 10 wt % $\text{V}_2\text{O}_5/\text{Al}_2\text{O}_3$ ($8.0 \text{ V}/\text{nm}^2$) [14 kPa C_2H_6 or C_2D_6 , 1.7 kPa O_2 , 663 K].

OH^* , and $*$ in the order in which they appear. Table 2 contains α and β , which are the collected equilibrium and rate parameters preceding the OH^* and $*$ terms, ($K_1^{0.25} k'_2^{0.25} K_4^{-0.5} 2k_5^{-0.25}$ and $K_1^{0.5} k'_2^{0.5} 2k_5^{-0.5}$, respectively). The values of α and β , when multiplied by typical reactant and product concentrations, are small relative to the 1 in this denominator, suggesting that the concentrations of OH^* and $*$ are small compared to that of O^* . The calculated values for OH^* and $*$ are qualitatively consistent with our recent in situ measurements of the number reduced vanadia centers using UV-vis spectroscopy, which suggest that $< \sim 5\%$ of the vanadium atoms are reduced during steady-state alkane ODH reactions.²⁰ At low reaction temperatures, the value of α leads to OH^* surface coverage estimates of $\sim 8\%$, which are consistent with the mild inhibition effects of water observed on ethane ODH rates (Figure 3). These inhibition effects weaken with increasing temperature because of the exothermic nature of the water adsorption step, which titrates vacancy sites ($*$) with OH^* and decreases the number of lattice oxygen atoms (O^*) available for kinetically relevant C-H bond activation steps.

Isotopic Tracer Studies and Kinetic Isotopic Effects. The kinetic significance and reversibility of the elementary steps shown in Scheme 2 and the role of lattice oxygen atoms in C-H bond activation were probed using reactants and products labeled with ^2H , ^{13}C , or ^{18}O . Kinetic isotope effects were measured from separate reactions of $\text{C}_2\text{H}_6-\text{O}_2$ and $\text{C}_2\text{D}_6-\text{O}_2$ reactant mixtures (14 kPa ethane; 1.7 kPa O_2) on 10 wt % $\text{V}_2\text{O}_5/\text{Al}_2\text{O}_3$. Several of these experiments were repeated on 10 wt % $\text{V}_2\text{O}_5/\text{ZrO}_2$, with similar conclusions.

Figure 5 shows ethene formation rates from $\text{C}_2\text{H}_6-\text{O}_2$ and $\text{C}_2\text{D}_6-\text{O}_2$ mixtures at 663 K as a function of reactor residence

**Figure 6.** **a.** Deuterium distribution in ethane during ODH of $\text{C}_2\text{H}_6-\text{C}_2\text{D}_6-\text{O}_2$ mixtures on 10 wt % $\text{V}_2\text{O}_5/\text{Al}_2\text{O}_3$ ($8.0 \text{ V}/\text{nm}^2$); squares: starting mixture; circles: 2.5 h reaction time, 4.4% ethane conversion; dashed line represents binomial distribution [6.8 kPa C_2H_6 , 6.8 kPa C_2D_6 , 1.7 kPa O_2 , 663 K, recirculating batch reactor]. **b.** Deuterium distribution in ethane formed from $\text{C}_2\text{H}_6-\text{C}_2\text{D}_6-\text{O}_2$ mixtures on 10 wt % $\text{V}_2\text{O}_5/\text{Al}_2\text{O}_3$ ($8.0 \text{ V}/\text{nm}^2$); dashed line represents binomial distribution [6.8 kPa C_2H_6 , 6.8 kPa C_2D_6 , 1.7 kPa O_2 , 663 K, recirculating batch reactor, 2.5 h reaction time, 4.4% ethane conversion].

time. The primary C_2H_6 dehydrogenation rate constant ($k_{1\text{H}}$) obtained from these data is 2.4 times larger than the rate constant for C_2D_6 dehydrogenation ($k_{1\text{D}}$). This normal kinetic isotope effect (KIE) is consistent with kinetically relevant C-H bond activation steps (Step 2 in Scheme 2), as assumed in most previous studies.^{1-5,8,12} The KIE for each of the reactions in Scheme 1 is discussed in greater detail below. At $< 3\%$ ethane conversion, the rates of ethene formation presented in Figure 5 decreased with increasing contact time to an extent much greater than expected from the slight depletion of the ethane reactants. This decrease in the net rate of ethene formation reflects the combustion (via Reaction 3 in Scheme 1) of some of the ethene formed in primary ODH steps, as well as a weak inhibition of ethane ODH rates by the water formed in ODH and combustion steps (Figure 3).

A $\text{C}_2\text{H}_6-\text{C}_2\text{D}_6-\text{O}_2$ (6.8-6.8-1.7 kPa) mixture was used in order to examine the reversibility of C-H bond activation steps (Step 2). $\text{C}_2\text{H}_6-x\text{D}_x$ isotopomers would be expected to form if this step were reversible. Figure 6a shows that equimolar C_2H_6-

C_2D_6 reactant mixtures did not lead to detectable amounts of mixed $C_2H_{6-x}D_x$ isotopomers, consistent with irreversible C–H bond activation steps. Mathematical instabilities in the matrix inversion procedures used to calculate isotopomer distributions and weak secondary kinetic isotope effects in mass fragmentation patterns lead to the observed scatter in isotopomer concentrations (around zero) and to slightly negative values for some of the mixed isotopomers. No mixed isotopomers of ethene ($C_2H_{4-x}D_x$) were detected (Figure 6b), indicating that hydrogen abstraction steps in ethoxide groups (to form ethene) are also irreversible and that the reversible readsorption of ethene on OH^* , via the microscopic reverse of ethene formation from ethoxide species, is slow relative to ethane ODH turnovers. It appears that the readsorption of ethene on O^* sites and the concomitant C–H bond activation required for secondary ethene reactions to form CO_x are also irreversible and that the cleavage of the first C–H bond in ethene leads to rapid cascade reactions leading to the ultimate desorption of CO and CO_2 . The amount of C_2H_4 formed is larger than that of C_2D_4 for equimolar C_2H_6 – C_2D_6 reactant mixtures because normal kinetic isotope effects favor ODH reactions of C_2H_6 over those of C_2D_6 (by a factor of 2.4).

A C_2H_6 – O_2 – D_2O (13.5–1.7–0.5 kPa) reactant mixture was used in order to confirm the irreversibility of Steps 2 and 3 and to determine the extent to which OH^* recombination steps leading to H_2O desorption (Step 4) are reversible. Neither $C_2H_{6-x}D_x$ nor $C_2H_{4-x}D_x$ were detected (Figure 7a and 7b), consistent with irreversible C–H bond activation steps in both ethane and ethene molecules. A binomial distribution of H_2O , HDO, and D_2O isotopomers indicates that quasi-equilibrium between OH^* and $H_2O_{(g)}$ is achieved during ethane ODH reactions. Previous studies using C_3H_8 – O_2 – D_2O mixtures have also concluded that water desorption steps are reversible,¹² but rapid isotopic exchange unrelated to propane dehydrogenation steps prevented a definite assessment of the extent of reversibility. OH recombination steps must be reversible for H_2O to be able to inhibit ODH rates, as observed for propane^{12–14} and ethane (Figure 3) reactions. Irreversible H_2O desorption steps would prevent gas-phase H_2O molecules from influencing the surface concentration of any adsorbed intermediates or the rate of any surface reactions.

Figure 8a shows the ^{18}O isotopic content in the water formed from C_2H_6 – $^{18}O_2$ – $^{16}O_2$ reactant mixtures on a VO_x/Al_2O_3 (10 wt % V_2O_5 , 8.0 V/nm^2) sample containing only ^{16}O . The initial H_2O products formed contained predominately ^{16}O from the VO_x lattice and only trace amounts of ^{18}O from the $^{18}O_2$ – $^{16}O_2$ equimolar reactant mixture. This suggests that lattice oxygen is involved in the activation of C–H bonds in ethane and in the primary formation of water via Step 4 (in Scheme 2). As catalytic turnovers occur, lattice ^{16}O is gradually removed as $H_2^{16}O$ and replaced with equimolar amounts of ^{18}O and ^{16}O from O_2 via the filling of vacancies in Step 5 (Scheme 2). As a result, the $H_2^{16}O/H_2^{18}O$ ratio increases with reaction time and approaches the value of unity expected from the equimolar amounts of ^{18}O and ^{16}O atoms in the reactant stream (Figure 8a). These conclusions, however, are not unequivocal, because the reversibility of water formation steps (Step 4) can lead to rapid isotopic exchange of any H_2O formed with the pool of lattice ^{16}O pool via the reverse of Step 4.

No $^{18}O^{16}O$ isotopomers were detected in the reactor effluent at any conversion or contact time (Figure 8a) during reactions of C_2H_6 – $^{18}O_2$ – $^{16}O_2$ reactant mixtures. Reversible O_2 dissociation steps (Step 5) would lead to mixed dioxygen isotopomers, as the recombination of lattice oxygen species occurs more

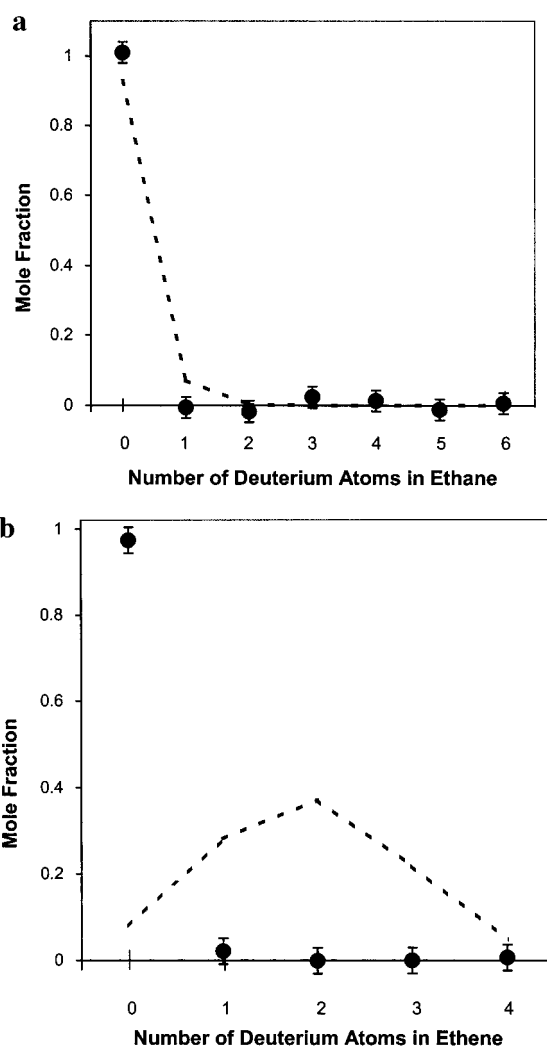


Figure 7. a. Deuterium distribution in ethane during reaction of C_2H_6 – O_2 – D_2O mixtures on 10 wt % V_2O_5/Al_2O_3 (8.0 V/nm^2); dashed line represents binomial distribution [14 kPa C_2H_6 , 1.7 kPa O_2 , 0.5 kPa D_2O , 663 K, recirculating batch reactor, 3.1 h reaction time, 2.8% ethane conversion]. b. Deuterium distribution in ethene formed from C_2H_6 – O_2 – D_2O mixtures on 10 wt % V_2O_5/Al_2O_3 (8.0 V/nm^2); dashed line represents binomial distribution [14 kPa C_2H_6 , 1.7 kPa O_2 , 0.5 kPa D_2O , 663 K, recirculating batch reactor, 3.1 h reaction time, 2.8% ethane conversion].

rapidly than ODH turnovers. Thus, as also shown for propane ODH reactions on VO_x ^{12,13} and MoO_x ,¹³ O_2 dissociation steps are irreversible during ethane ODH on VO_x -based catalysts.

Figure 8b shows the $^{18}O/^{16}O$ isotopic ratio in the H_2O , CO, and CO_2 formed from the C_2H_6 – $^{18}O_2$ – $^{16}O_2$ reactant mixture. CO and CO_2 also contain only ^{16}O during the initial stages of the reaction, confirming that lattice oxygen is also involved in primary and secondary combustion reactions. The distribution of ^{18}O in the CO_2 is binomial, indicating that statistical sampling of lattice oxygen atoms occurs during CO_2 formation. The ^{18}O contents in H_2O , CO, and CO_2 are similar and increase concurrently with increasing reaction time as the lattice reaches equilibrium with the equimolar $^{16}O_2$ – $^{18}O_2$ reactant mixture and ultimately provides lattice ^{18}O and ^{16}O atoms with equal probability for both primary and secondary products. ODH and combustion reactions appear to sample the same lattice oxygen pool, suggesting that similar sites are involved in ODH and combustion reactions.

A reactant mixture consisting of C_2H_6 (14 kPa), $^{13}C_2H_4$ (0.5 kPa), and O_2 (1.7 kPa) was used in order to measure the relative

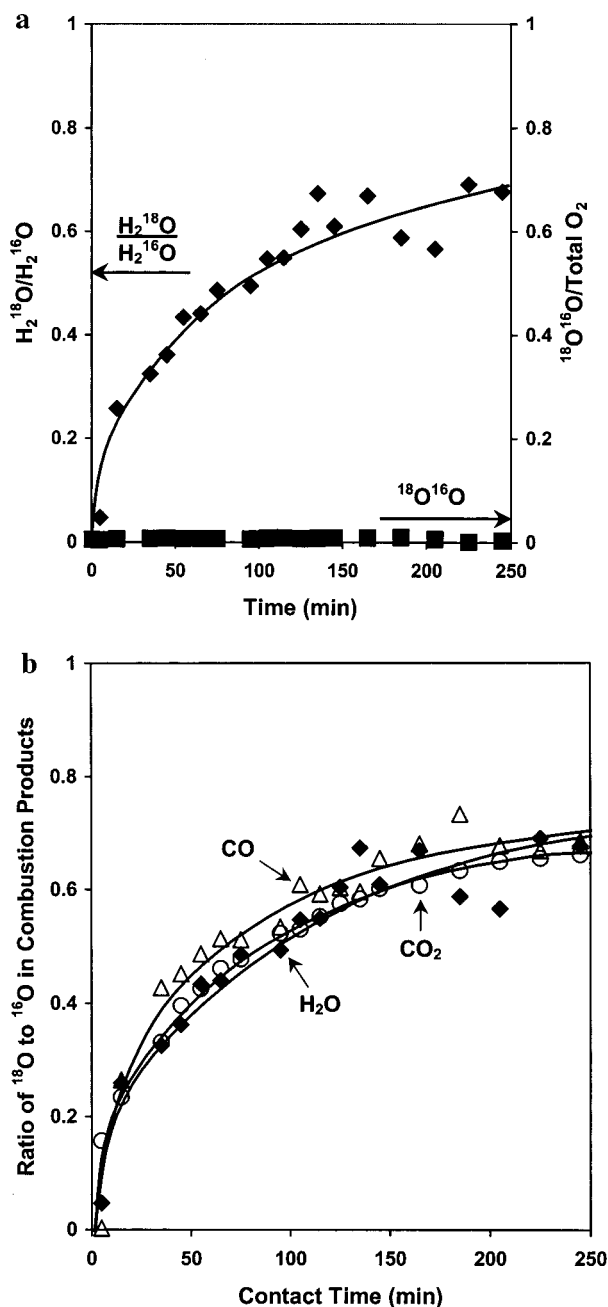


Figure 8. a. The time evolution of the $\text{H}_2^{18}\text{O}/\text{H}_2^{16}\text{O}$ ratio in the water product and of the $^{18}\text{O}^{16}\text{O}$ fraction in the O_2 reactant during the reaction of ethane and a mixture of $^{16}\text{O}_2$ – $^{18}\text{O}_2$ on 10 wt % $\text{V}_2^{16}\text{O}_5/\text{Al}_2^{16}\text{O}_3$ [14 kPa C_2H_6 , 0.85 kPa $^{16}\text{O}_2$, 0.85 kPa $^{18}\text{O}_2$, 663 K, recirculating batch reactor]. b. The time evolution of the $^{18}\text{O}/^{16}\text{O}$ content of all combustion products from the reaction of ethane and a mixture of $^{16}\text{O}_2$ – $^{18}\text{O}_2$ on 10 wt % $\text{V}_2^{16}\text{O}_5/\text{Al}_2^{16}\text{O}_3$ [14 kPa C_2H_6 , 0.85 kPa $^{16}\text{O}_2$, 0.85 kPa $^{18}\text{O}_2$, 663 K, recirculating batch reactor].

rates of primary and secondary reactions and the reversibility of the overall ethane dehydrogenation reaction at 663 K on $\text{VO}_x/\text{Al}_2\text{O}_3$ (10 wt %, 8.0 V/nm^2). These competitive reactions of C_2H_6 and $^{13}\text{C}_2\text{H}_4$ showed that CO and CO_2 form via direct ethane combustion and secondary ethene combustion reactions. The CO and CO_2 formed from C_2H_6 – $^{13}\text{C}_2\text{H}_4$ – O_2 mixtures showed similar ^{13}C contents at all contact times (Figure 9), suggesting that CO and CO_2 form from both C_2H_6 and $^{13}\text{C}_2\text{H}_4$. The initial concentration of $^{12}\text{C}_2\text{H}_6$ is 27 times greater than that of $^{13}\text{C}_2\text{H}_4$, but the initial ^{13}C fraction in CO_x combustion products, which form from essentially unscrambled reactants, is 0.47, indicating that rate constants of C_2H_4 combustion (k_3

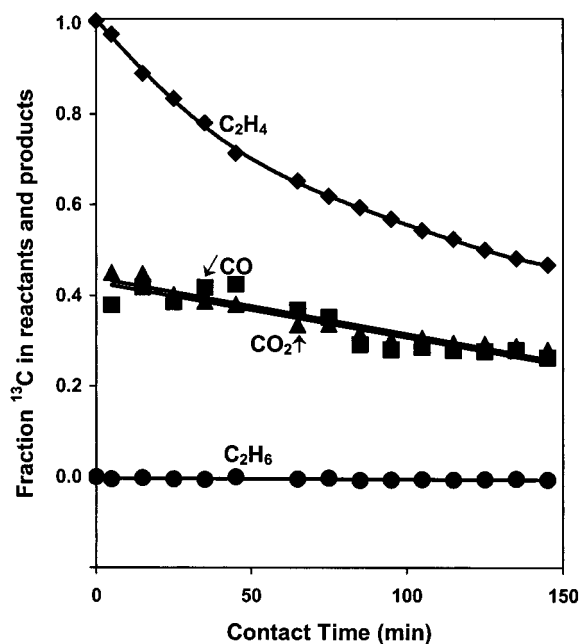


Figure 9. ^{13}C content of products during ethane ODH, with $^{13}\text{C}_2\text{H}_4$ initially present, on 10% $\text{VO}_x/\text{Al}_2\text{O}_3$, 8.0 V/nm^2 [14 kPa C_2H_6 , 1.7 kPa O_2 , 0.5 kPa $^{13}\text{C}_2\text{H}_4$, 663 K, recirculating batch reactor].

TABLE 3: Reaction Rate Constant k_1 , k_2 , and k_3 ($\text{cm}^3 \text{mol}^{-1} \text{s}^{-1}$) and Kinetic Isotope Effects on 10 wt % $\text{VO}_x/\text{Al}_2\text{O}_3$ Catalysts (14 kPa C_2H_6 or 14 kPa C_2D_6 , 1.7 kPa O_2 , Balance He, 663 K)

	ethane dehydrogenation (k_1)	ethane combustion (k_2)	ethene combustion (k_3)
$k_{i,\text{C-H}}$	30	10	170
$k_{i,\text{C-D}}$	12	5.3	61
$k_{i,\text{C-H}}/k_{i,\text{C-D}}$	2.4	1.9	2.8

in Scheme 1) are significantly larger than for C_2H_6 combustion (k_2 in Scheme 1) ($k_3/k_2 = 14$). The ^{13}C content in CO_x decreases with increasing contact time because unlabeled ethene formed from $^{12}\text{C}_2\text{H}_6$ dilutes the isotopically pure $^{13}\text{C}_2\text{H}_4$ reactants initially present. A kinetic analysis of these data shows that k_3 is 5.8 times greater than the rate constant of ethene formation (k_1 in Scheme 1). The k_2/k_1 ratio is 0.36, indicating a primary C_2H_4 selectivity of 74%. Both ratios agree with values of these rate constants obtained from the effects of reactor residence time on reaction rate and product selectivity in a flow reactor.¹¹ The value of k_3/k_2 obtained from the latter measurements was 16 (11), in excellent agreement with the value of 14 reported here from isotopic tracer studies. Figure 9 shows that no ^{13}C is detected in ethane even at ethane conversions of 4.4%, confirming the irreversible nature of C–H bond activation steps, also shown from C_2H_6 – C_2D_6 – O_2 (Figure 6) and C_2H_6 – O_2 – D_2O (Figure 7) experiments.

H–D Kinetic Isotope Effects for Primary and Secondary Reactions. Kinetic isotope effects (KIE) measured from reactions of C_2H_6 – O_2 and C_2D_6 – O_2 mixtures are shown in Table 3 for each reaction step in Scheme 1. Primary dehydrogenation (k_1), primary combustion (k_2), and secondary combustion (k_3) rate constants were extracted from these rate data as a function of reaction time on 10 wt % $\text{V}_2\text{O}_5/\text{Al}_2\text{O}_3$ at 663 K. As noted earlier (Figure 5), the kinetic isotope effect for ethane conversion to ethene ($k_{1\text{H}}/k_{1\text{D}}$) is 2.4, as expected for kinetically relevant steps involving C–H bond cleavage. The corresponding kinetic isotope effects are 1.9 for ethane combustion to CO and CO_2 ($k_{2\text{H}}/k_{2\text{D}}$) and 2.8 for ethene combustion ($k_{3\text{D}}/k_{3\text{H}}$). These normal

KIE are similar for all three steps, suggesting that C–H bond activation is a common requirement and a kinetically relevant step for all three reactions. These conclusions are reasonable in view of the similar site requirements exhibited by these primary and secondary pathways.^{1–4,11}

The KIE values reported here for ethane and ethene reactions resemble those reported recently for propane and propene reactions on VO_x/ZrO₂.^{12,14} For propane and propene reactions, KIE values were 2.5–2.8 for k_{1H}/k_{1D} , 1.7–1.9 for k_{2H}/k_{2D} , and 2.2–2.6 for k_{3D}/k_{3H} , all of which resemble the values reported here for C₂ reactions.

The different KIE values measured for alkane ODH, alkane combustion, and alkene combustion (for both C₂ and C₃) reflect the different extent to which the C–H bond is cleaved and the O–H and O–C bonds are formed in the transition state required for the C–H activation steps involved in each reaction. In the absence of concerted formation of O–H and O–C bonds using lattice oxygen atoms, KIE values would approach ~6 for ethane at 663 K.¹⁴ KIE values decrease when concerted formation of O–H or O–D bonds compensates in part for the higher bond energy of C–D bonds relative to C–H bonds. It appears that the involvement of lattice oxygen in the formation of transition states for alkane combustion is more extensive than for alkane ODH or alkene combustion, suggesting the involvement of specific lattice oxygen atoms with a somewhat higher affinity and reactivity for the formation of O–H bonds during C–H bond activation.

Conclusions

Oxidative dehydrogenation of ethane on VO_x/Al₂O₃ and VO_x/ZrO₂ occurs via parallel and sequential reactions, with ethene as the most abundant primary product. The assumption that surface oxygen, OH groups, and vacancies are the most abundant reactive intermediates leads to a rate equation that accurately describes measured ethane ODH reaction rates. The dependencies of these rates on C₂H₆, O₂, and H₂O concentrations are identical on supported VO_x and V₂O₅ powders, suggesting that similar active centers are present on both surfaces. C₂H₆–C₂D₆ and C₂H₆–D₂O reactants undergo ODH reactions without forming C₂H_{6–x}D_x or C₂H_{4–x}D_x mixed isotopomers, suggesting that C–H bond activation steps are irreversible. The absence of C₂H_{4–x}D_x mixed isotopomers suggests that activation of ethene C–H bonds leads only to combustion products. The normal kinetic isotopic effects measured for primary oxidative dehydrogenation reactions and for ethane and ethene combustion

steps support the kinetic relevance of C–H bond activation. Competitive reactions of ¹⁶O₂–¹⁸O₂–C₂H₆ mixtures on supported V¹⁶O_x lead to the preferential initial appearance of lattice ¹⁶O atoms in the product water, as expected if lattice oxygens were required for the activation of C–H bonds, but this conclusion is not unequivocal because water formation steps are reversible and can lead to isotopic scrambling between water and lattice oxygens. The labeled oxygen content is identical for H₂O, CO, and CO₂, suggesting that the same lattice oxygen pool and active sites are involved in the kinetically relevant C–H activation steps involved in ODH and combustion reactions.

Acknowledgment. This work was supported by the Director, Office of Basic Energy Sciences, Chemical Sciences Division of the U.S. Department of Energy under Contract DE-AC03-76SF00098.

References and Notes

- (1) Kung, H. H. *Adv. Catal.* **1994**, *40*, 1.
- (2) Mamedov, E. A.; Cortés Corberán, V. *Appl. Catal. A* **1995**, *127*, 1.
- (3) Albonetti, S.; Cavani, F.; Trifirò, F. *Catal. Rev.—Sci. Eng.* **1996**, *38*, 413.
- (4) Blasco, T.; López Nieto, J. M. *Appl. Catal. A* **1997**, *157*, 117.
- (5) Hong, S. S.; Moffat, J. B. *Appl. Catal. A* **1994**, *109*, 117.
- (6) Zhao, Z.; Yamada, Y.; Teng, Y.; Ueda, A.; Nakagawa, K.; Kobayashi, T. *J. Catal.* **2000**, *190*, 215.
- (7) Le Bars, J.; Védrine, J. C.; Auroux, J. A.; Trautmann, S.; Baerns, M. *Appl. Catal. A* **1992**, *88*, 179.
- (8) Oyama, S. T. *J. Catal.* **1991**, *128*, 210.
- (9) Oyama, S. T.; Middlebrook, A. M.; Somorjai, G. A. *J. Phys. Chem.* **1990**, *94*, 5029.
- (10) Thorsteinson, E. M.; Wilson, T. P.; Young, F. G.; Kasai, P. H. *J. Catal.* **1978**, *52*, 116.
- (11) Argyle, M. D.; Chen, K. D.; Bell, A. T.; Iglesia, E. *J. Catal.*, in press.
- (12) Chen, K. D.; Khodakov, A.; Yang, J.; Bell, A. T.; Iglesia, E. *J. Catal.* **1999**, *186*, 325.
- (13) Chen, K. D.; Bell, A. T.; Iglesia, E. *J. Phys. Chem. B* **2000**, *104*, 1292.
- (14) Chen, K. D.; Iglesia, E.; Bell, A. T. *J. Catal.* **2000**, *192*, 197.
- (15) Mars, P.; van Krevelen, D. W. *Chem. Eng. Sci. (Special Suppl.)* **1954**, *3*, 41.
- (16) Khodakov, A.; Yang, J.; Su, S.; Iglesia, E.; Bell, A. T. *J. Catal.* **1998**, *177*, 343.
- (17) Khodakov, A.; Olthof, B.; Bell, A. T.; Iglesia, E. *J. Catal.* **1999**, *181*, 205.
- (18) Iglesia, E.; Baumgartner, J. E.; Price, G. L. *J. Catal.* **1992**, *134*, 549.
- (19) Price, G. L.; Iglesia, E. *Ind. Eng. Chem. Res.* **1989**, *28*, 839.
- (20) Argyle, M. D.; Chen, K. D.; Iglesia, E.; Bell, A. T. Unpublished results.